DEPT. OF MATH. UNIVERSITY OF OSLO
MECHANICS AND APPLIED MATHEMATICS NO. 1
ISSN 0809–4403 JUNE 2004

Analysis of current and sea level observations from Trondheimsleia

Steinar Orre[1], Espen Åkervik[2] and Bjørn Gjevik[3]

June 22, 2004

Abstract

Sea level and current measurements from Trondheimsleia have been analysed and the parameters of the tidal ellipses for the major tidal components M_2, S_2, N_2, and K_1 have been calculated. Harmonic constants for sea level and tidal ellipse parameters have been compared with the corresponding data from a high resolution tidal model in order to validate the performance of the model. Short periodic oscillations with period about 40 minutes are observed at the time of peak tidal current at one station with relatively strong tidal currents in the channel between Storfosna and Garten.

1 Introduction

The main objectives of a research project funded by The Norwegian Research Council under the BeMatA program have been to develop a high resolution tidal model for a section of the Norwegian coast, called Trondheimsleia, and to implement the current fields in the electronic chart display and information system (ECDIS) (Gjevik et al. 2004). For validation of the performance of the tidal model observational data from a series of stations with sea level and current measurements have been used. This report discribes the analysis of the observational data and the comparison with model data. The observational data come from two separate field campaigns. The first from December 2001 to February 2002 where sea level was recorded at six stations by the Norwegian Hydrographic Service (Hareide & Lynge 2002). The second campaign took place in two periods from January to March 2002 where currents were recorded at 18 stations along a proposed pipeline track from Tjeldbergodden to Skogn in the inner part of Trondheimsleia for Statoil.

[1]Nansen Environmental and Remote Sensing Center, Thormøhlensgate 47, N-5006 Bergen, Norway
[2]Department of Mechanics, Kungliga Tekniska Högskolan, SE-100 44 Stockholm, Sweden
[3]Department of Mathematics, University of Oslo, P.O.Box 1053 Blindern, N-0316 Oslo, Norway

2 Models

2.1 The regional model

In a report by Moe, Gjevik & Ommundsen (2003) presented the results of a numerical model, for simulating tides on a section of the shelf off the coast of Møre and Trøndelag in western Norway with 500 m grid resolution. The equations solved are the depth integrated shallow water equations (SWE), with linearized advection terms:

$$\begin{aligned} \frac{\partial \eta}{\partial t} &= -\frac{\partial U}{\partial x} - \frac{\partial V}{\partial y} \\ \frac{\partial U}{\partial t} - fV &= -gH\frac{\partial \eta}{\partial x} - c_D\frac{\sqrt{U^2+V^2}}{H}\frac{U}{H} \\ \frac{\partial V}{\partial t} + fU &= -gH\frac{\partial \eta}{\partial y} - c_D\frac{\sqrt{U^2+V^2}}{H}\frac{V}{H} \end{aligned} \tag{1}$$

where (U, V) specify the components of volume flux vector per unit length in the horizontal plane, η the vertical displacement of the sea surface from the mean sea level, $H = H_0 + \eta$ the total depth, H_0 the mean depth, g acceleration of gravity, f the Coriolis parameter, c_D the drag coefficient of the quadratic bottom shear stress. For the full model setup and the results of the simulations we refer to the original paper. Simulations for the coasts of Møre and Trøndelag in Mid-Norway yielded harmonics constants for the semi-diurnal components M_2, S_2, N_2 and the diurnal component K_1. The results of this model have been used to calculate, by interpolation, the boundary conditions along the open boundaries for a high resolution model for Trondheimsleia.

2.2 The high resolution model for Trondheimsleia

The harmonic constants used in the comparisons were obtained by simulations with a 100 m grid resolution model, covering Trondheimsleia (Gjevik et. al 2004). We shall subsequently refer to this model as HRMT. The model domain is depicted in figure 1. This model uses interpolated harmonic constants from Moe et al. (2003) as boundary input. The depth matrix was calculated for an UTM coordinate grid (with $\Delta x = \Delta y = 0.1$ km) based on multi-beam bathymetric soundings and high resolution hydrographic surveys by The Norwegian Hydrographic Service (NHS), Stavanger. Data files with the resulting harmonic constants for the M_2, S_2, N_2 and K_1 tidal components both for the sea-elevation (η) and the components of the depth mean currents ($\bar{u} = U/H_0$ and $\bar{v} = V/H_0$) are available on the web site: enlil.uio.no:/work/atleo/halten/mach/. Data for the components M_2 and S_2 are found under `run102`, and for N_2 and K_1 under `run104`. These data sets are used subsequently in this report for comparison with field data. The modelled current fields have also been used to calculate dispersion and mixing in the tidal field (Orre 2004).

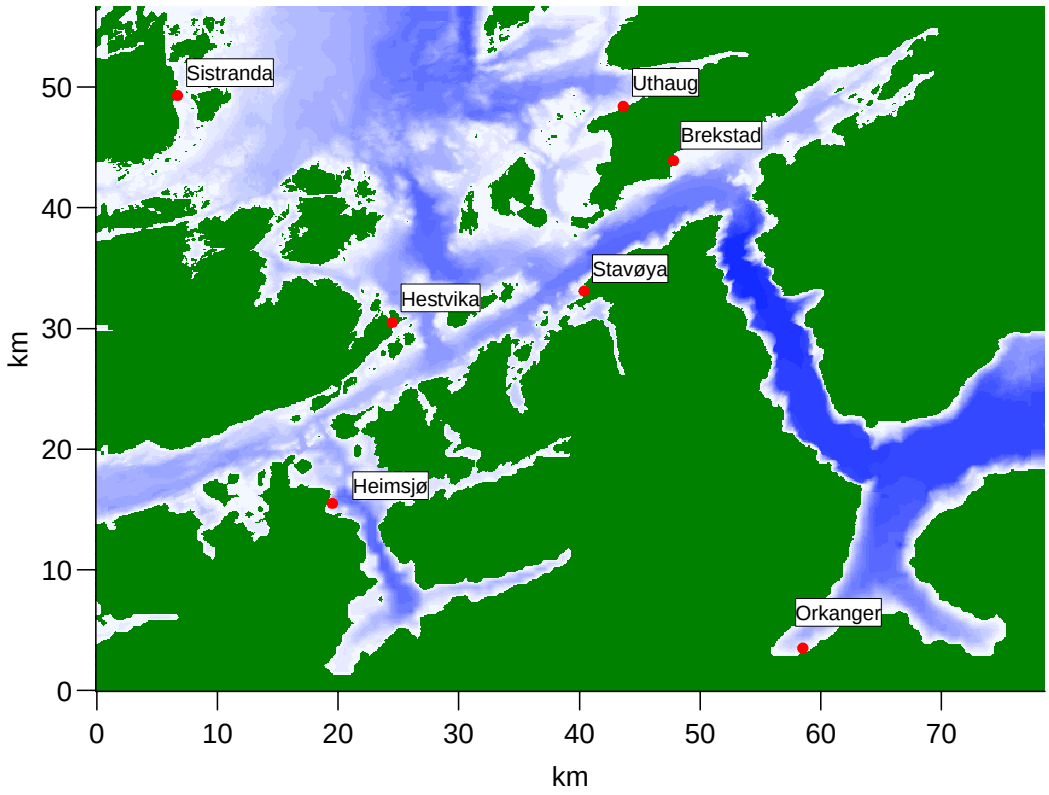

Figure 1: The model domain of the high resolution model for Trondheimsleia, the locations of the stations with sea level observations are depicted.

3 Sea level observations and comparison with model data

3.1 Measurements

The Norwegian Hydrographic Service (NHS) conducted sea level observations in Trondheimsleia and Frohavet for validation of the HRMT model, see the report of Hareide & Lynge (2002). Five temporary tide gauges and one permanent tide station located inside the model domain have been used for this purpose, see Figure 1. The exact position of the temporary gauges are given in Table 1. The data from Orkanger (only M_2) are from earlier measurements. At the stations located at Uthaug, Sistranda and Hestvika a WLR7 (Water Level Recorder 7) manufactured by Aanderaa Instruments was used. This instrument measures pressure, temperature and conductivity at regular time intervals. On basis of these data and barometric pressure, variation in water level is calculated. All data is stored directly into the local data storing unit inside the instrument. At the two other temporary stations Agdenes (Stavøya) and Brekstad, a smaller mobile tide gauge was used; the Sutron mobile tide gauge with a pressure transducer from Pressure Systems Inc., USA. The station located at Heimsjø is one of the permanents stations along the Norwegians coast (called the MDS tide gauge network), and all of these stations are equipped with a Sutron datalogger. During operation the sea level data from the datalogger inside the Sutron tide gauge are transmitted to the

central computer at NHS once every night. The five temporary tide gauges were deployed in the beginning of December 2001 and recovered mid February 2002 by staff from NHS.

For comparison with the HRMT model, data from model gridpoints near the stations have been used, positions are given in Table 2 and indicated on the map in Figure 1. We emphasize that the locations of the model gridpoint are not identical with the locations of the gauges used for observations, the grid point representing Heimsjø is actually a few gridpoints off-shore, while the recorder is located at the shore line. It has been checked that the variation in sea level is small in this area and that the model data from the grid points near the stations are representative for comparison of model and observational data.

Table 1: List of the stations with sea level observation; location in geographical coordinates and sensor type.

Station	*Geographical coordinates*	*Sensor*
Hestvika	N 63^o 34' 4.17" E 09^o 11' 58.28"	WLR
Uthaug	N 63^o 43' 39.6" E 09^o 35' 19.50"	WLR
Brekstad	N 63^o 41' 13.2" E 09^o 40' 10.70"	Sutron
Stavøya	N 63^o 35' 27.9" E 09^o 31' 13.27"	Sutron
Sistranda	N 63^o 44' 13.3" E 08^o 50' 22.90"	WLR

Table 2: List of model gridpoints near the recording stations used for model validation; water depth and location in UTM coordinates.

Station	*Depth (m)*	*UTM coordinates (m)*
Heimsjø	338	7034045.00N, 505823.63E
Hestvika	55	7048872.61N, 509909.50E
Uthaug	83	7066801.84N, 529076.67E
Brekstad	50	7062309.96N, 533118.92E
Stavøya	82	7051553.46N, 525822.66E
Sistranda	10	7067720.90N, 492085.50E
Orkanger	14	7021340.50N, 543425.25E

3.2 Comparison with model data

In Table 3, 4, 5, and 6 we present harmonic constants calculated from the observed sea level data from 7 locations in Trondheimsleia by NHS ((Hareide & Lynge 2002)) and corresponding data from the HRMT model. The harmonic constants presented in the column labeled Observations 1 are calculated from time series of different lengths. For example the data from Heimsjø are calculated from a 10 year long record of observation. The data from Orkanger is from a relatively short observation period of about one month. The data in the

Observation 2 column are calculated from the same observation period i. e. 15th of January to 17th of February 2002. The Model 1 is the standard data set (see section 2.2) while the model 2 data are obtained from a simulation with adjusted boundary conditions (Gjevik et al. 2004).

The time zone used in the harmonic analysis from NHS is in Middle European Time, MET (UT + 1 hour), while the HRMT model makes use of Universal Time, UT. For the sake of convenience; all the phase values presented in the following refer to UT.

Table 3: Harmonic constants for M_2

Station	*Observation 1*		*Observation 2*		*Model 1*		*Model 2*	
	H (cm)	$\delta(^0)$	H (cm)	$\delta(^0)$	H (cm)	$\delta(^0)$	H (cm)	$\delta(^0)$
Heimsjø	77.8	301	76.6	300	76.3	296	77.4	301
Hestvika	79.6	304	78.9	303	77.9	299	78.4	302
Uthaug	76.8	303	76.8	303	76.9	300	76.9	303
Brekstad	86.3	306	86.0	306	83.5	299	84.3	303
Stavøya	81.1	304	81.3	304	80.0	298	80.6	303
Sistranda	77.0	303	76.5	303	75.8	299	76.3	303
Orkanger	87.4	306			88.8	298	90.2	303

Table 4: Harmonic constants for S_2

Station	*Observation 1*		*Observation 2*		*Model 1*	
	H (cm)	$\delta(^0)$	H (cm)	$\delta(^0)$	H (cm)	$\delta(^0)$
Heimsjø	26.9	339	28.0	339	26.1	336
Hestvika	29.3	341	28.8	342	26.6	338
Uthaug	28.1	342	28.1	342	26.2	339
Brekstad	32.0	344	31.5	344	28.8	338
Stavøya	29.7	343	29.7	343	27.5	338
Sistranda	28.2	340	28.0	341	25.8	338

Table 5: Harmonic constants for N_2

Station	*Observation 1*		*Observation 2*		*Model 1*	
	H (cm)	$\delta(^0)$	H (cm)	$\delta(^0)$	H (cm)	$\delta(^0)$
Heimsjø	15.7	278	15.5	279	16.5	284
Hestvika	16.2	281	16.0	281	16.9	286
Uthaug	15.7	281	15.7	281	16.7	287
Brekstad	17.3	283	17.6	283	18.0	287
Stavøya	16.6	282	16.5	282	17.3	286
Sistranda	15.6	281	15.6	281	16.5	286

Table 6: Harmonic constants for K_1

Station	*Observation 1*		*Observation 2*		*Model 1*	
	H (cm)	$\delta(^0)$	H (cm)	$\delta(^0)$	H (cm)	$\delta(^0)$
Heimsjø	6.3	165	6.2	169	8.1	158
Hestvika	6.4	166	6.6	169	8.3	159
Uthaug	6.3	173	6.3	173	8.3	160
Brekstad	6.5	170	6.8	171	8.5	159
Stavøya	6.5	171	6.5	170	8.4	159
Sistranda	6.4	165	6.7	168	8.3	160

4 Current observations and comparison with model data

4.1 Measurement programme

In January 2002, Thales Geosolutions Norge AS performed an oceanographic survey in Trondheimsleia for Statoil ASA. The measurements were made along the proposed pipeline route from Tjeldbergodden to Skogn east of Trondheim, in water depths ranging from 30 to 590 m. A total of 18 sampling stations were initially selected, see Table 7 and Figure 2. Most of the measurements were made by sensors located near the sea bed. The first period of measurements was from the 9th of January to the 8th of March, and the second started 8th of March and ended 10th of May. The data from the first period and a short description of the program is presented in the report of Krug (2002). The data from the second period were available to us only as digital data files.

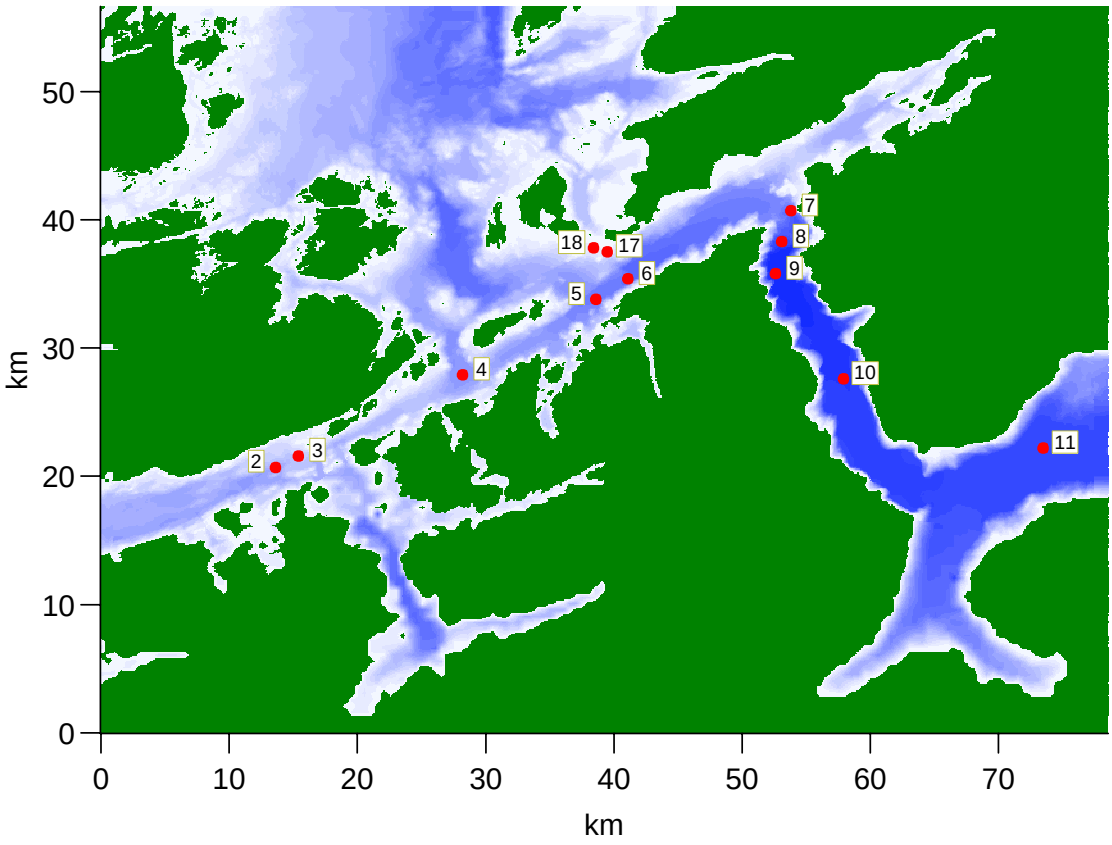

Figure 2: Location of the stations with current measurements within the model domain in Trondheimsleia. Stations 1, 12, 13, 14, 15, and 16 are outside the domain.

At all stations, ocean currents were measured with Aanderaa RCM7 (Recording Current Meters). The RCM7 is a self-contained instrument that can be moored in the sea and record ocean current, water temperature, conductivity of the water and instrument depth. At two of the sampling sites, an ADCP from RD Instruments were deployed to provide vertical

profile of the current. An Acoustic Doppler Current Profiler (ADCP) measures a vertical profile of horizontal current velocity. The instrument carries its own sound sources (sonar). It measures the time it takes for a sound signal to travel from the source, being reflected at a particular distance and then travel back to the source. By combining three (or more) such sonars, any motion relative to the sensor can be calculated according to the acoustic Doppler principle. ADCP usually give reliable results down to 2-400 meters, depending on the model. The RCM7 sensor were usually set 3 metres above the bottom, while the ADCP sensor samples currents for each 20 metres in the vertical column. Quality control on the current data were made, comprised a visual examination of the data, and a check for timing error. For example, if the current speed exceeded 5 m/s, or if one of the velocity components was unchanged over 3 bins in a depth profile, special care was taken (Krug 2002).

Harmonic analysis of the current data were made to provide harmonic constants (amplitude and phase) for each station, and for each tidal constituent. A total of 35 tidal constituents were included in the harmonic analysis, although we only make use of M_2, S_2, N_2 and K_1 in our analysis and comparison with model data. In the report of Krug (2002), harmonic constants for these four tidal constituents along with O_1 are presented.

Table 7: List of the 18 stations in Trondheimsleia; water depth, location in UTM and Geographical coordinates, and Sensor type.

St.	*Depth*	*UTM*	*Geographical*	*Sensor*
1	220	7034404.77N, 484826.64E	63.43625N, 08.69591E	RCM
2	220	7039142.54N, 499017.49E	63.47909N, 08.98028E	RCM
3	115	7039950.36N, 500831.34E	63.48634N, 09.01669E	RCM
4	275	7046253.57N, 513769.86E	63.54264N, 09.27699E	RCM
5	360	7052204.43N, 523957.61E	63.59550N, 09.48282E	RCM, ADCP
6	410	7053789.25N, 526504.40E	63.60954N, 09.53441E	RCM
7	430	7059116.00N, 539214.00E	63.65616N, 09.79198E	RCM, ADCP
8	520	7056651.96N, 538545.26E	63.63412N, 09.77787E	RCM
9	590	7054242.05N, 538039.94E	63.61255N, 09.76709E	RCM
10	550	7045950.17N, 543306.89E	63.53754N, 09.87101E	RCM
11	500	7040603.24N, 558891.51E	63.48732N, 10.18240E	RCM
12	40	7051253.00N, 576642.00E	63.57947N, 10.54381E	RCM
13	190	7055341.00N, 578215.00E	63.61580N, 10.57751E	RCM
14	420	7062085.70N, 586625.92E	63.67434N, 10.75078E	RCM
15	220	7067744.62N, 600776.40E	63.72133N, 11.04022E	RCM
16	30	7066970.45N, 603624.02E	63.71356N, 11.09731E	RCM
17	80	7055867.14N, 524945.06E	63.62830N, 09.50330E	RCM
18	50	7056237.13N, 523787.41E	63.63170N, 09.48000E	RCM

4.2 3-D plots of bottom topography

In order to visualize the bottom topography around the stations with current measurements we have generated a series of 3-D bathymetric plots, using the bathymetric database with 100m spatial resolution. This depth matrix was used for the model simulation.

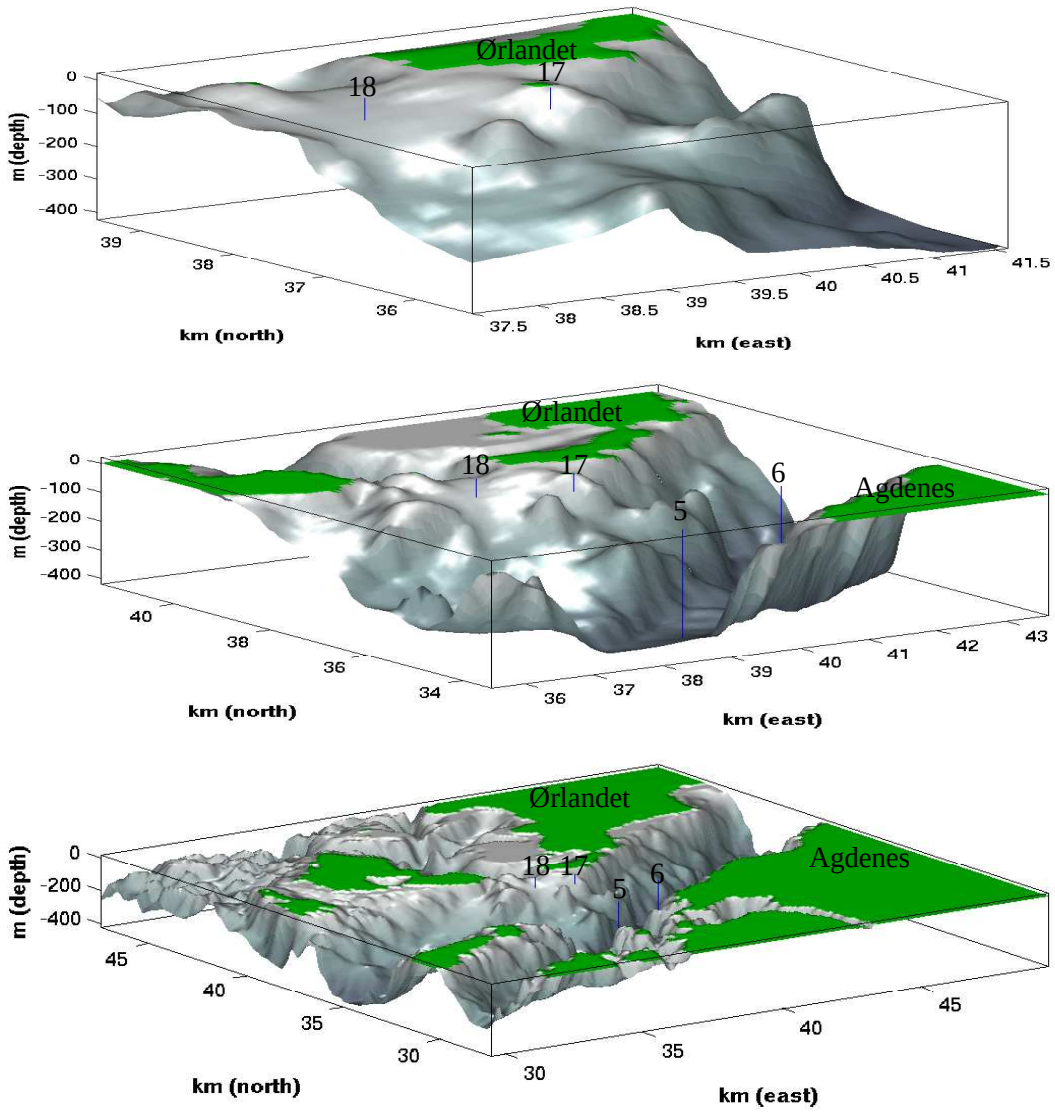

Figure 3: 3-D plots of bottom topography around stations 17, 18 and 6. The upper, mid and lower panel cover horizontal areas of 5×5 km, 8×8 km and 20×20 km centered around station 17.

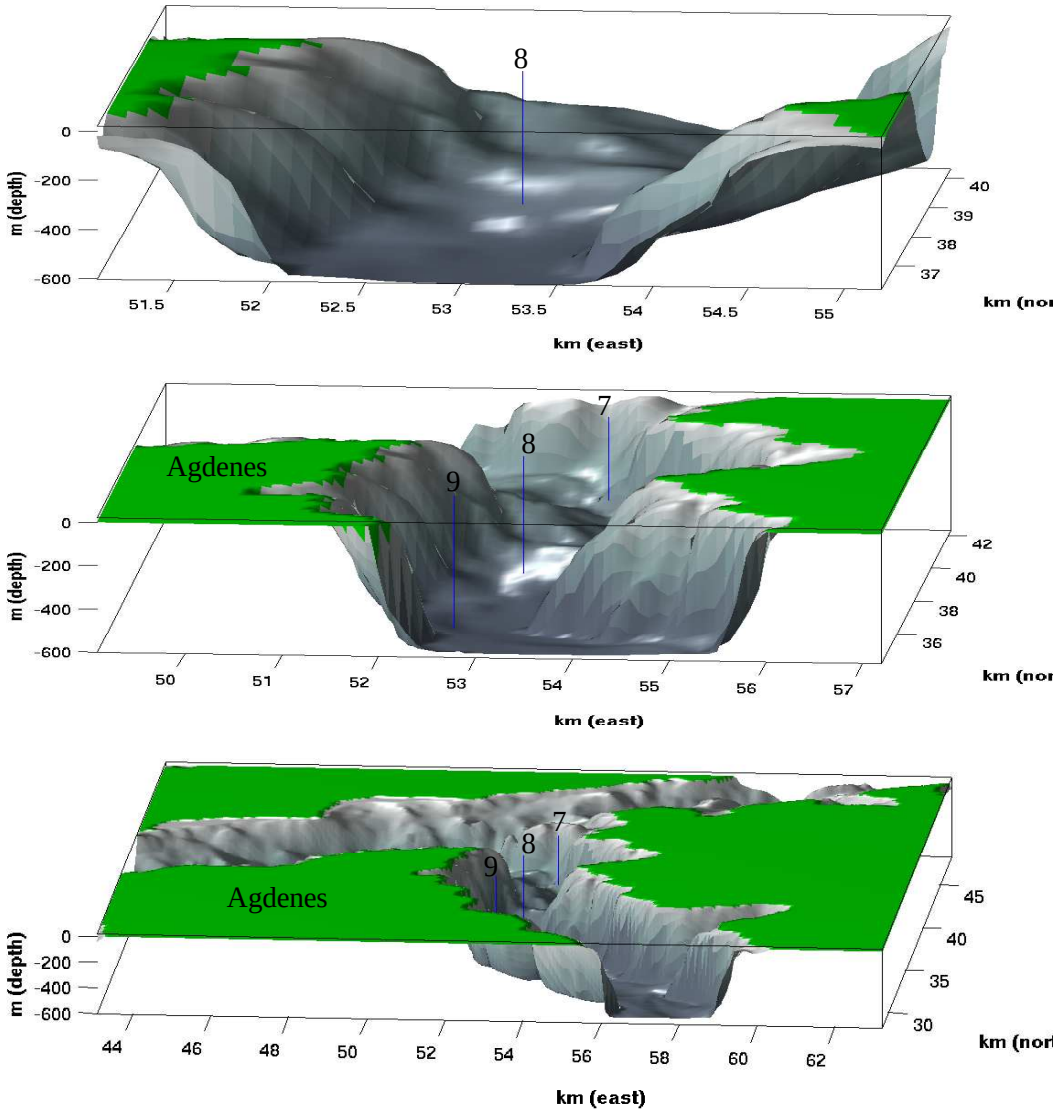

Figure 4: 3-D plots of bottom topography around stations 7 , 8 and 9. The upper, mid and lower panel cover horizontal areas of 5×5 km, 8×8 km and 20×20 km centered around station 8.

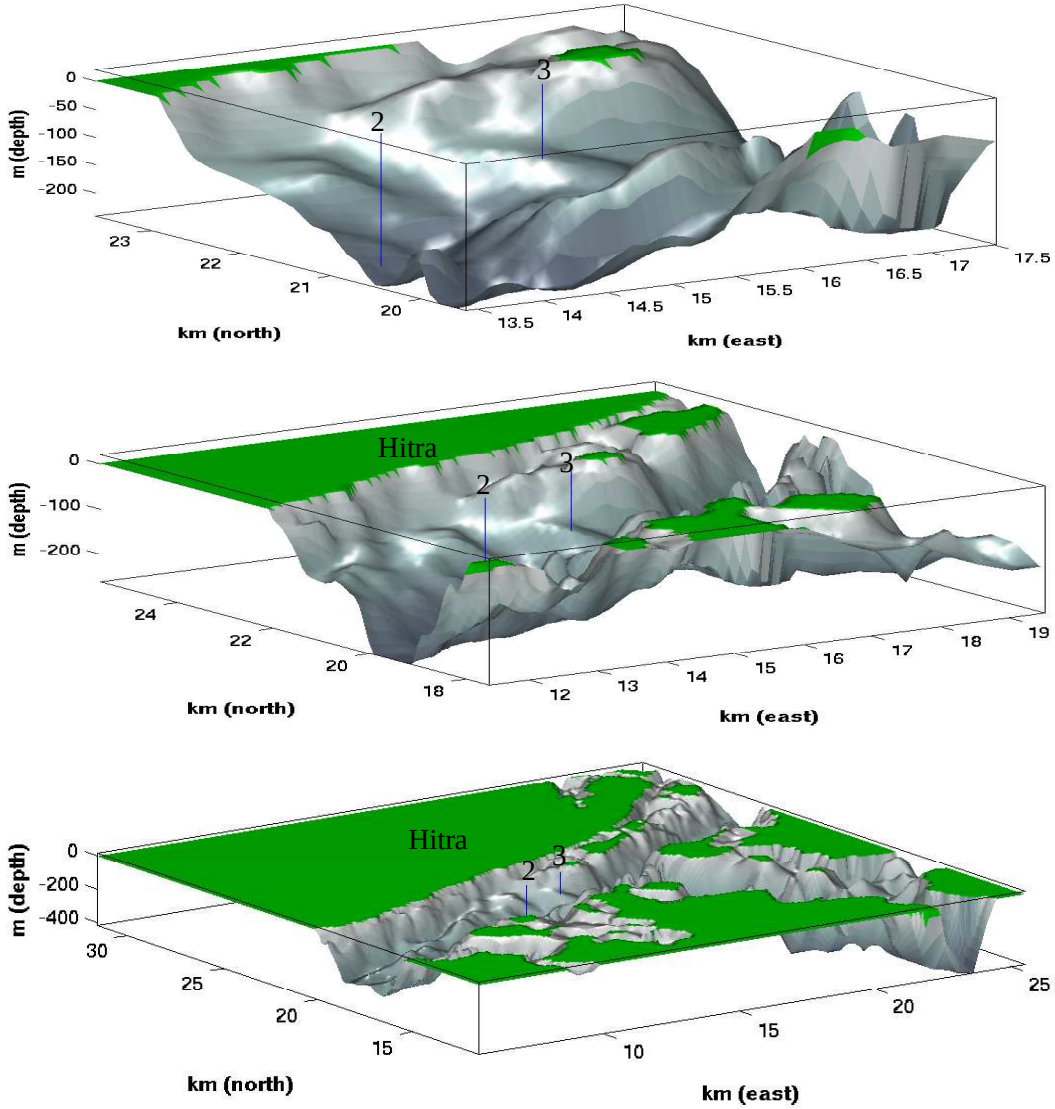

Figure 5: 3-D plots of bottom topography around stations 2 and 3. The upper, mid and lower panel cover horizontal areas of 5×5 km, 8×8 km and 20×20 km centered around station 3.

4.3 Comparison with model data

The output of the tidal model is presented as current ellipse parameters (ep-parameters). The observationed data by Krug (2002) are given as current amplitude and phase lag parameters (ap-parameters); and we have converted the ap-parameters to ep-parameters. For this conversion we used the MATLAB-scripts written by Xu (2002). Some care had to be taken, however, since there apparently exists different conventions for the definition of the inclination and rotation direction. In the report of Xu (2002), the inclination is defined as the angle between east and semi-major axis, while the definition in the article of Moe et al. (2003) inclination is the angle between the true north and the direction of the semi-major axis. In this report we make use of the latter definition of direction.

During the recording period, RCM data from some stations were lost due to various technical problems with the instruments. Other data sets were also taken out after running a quality control. In the presentation here, the measurement data are therefore incomplete; station 6 is not presented at all, while station 1, 4, 9, 17, and 18 only contain data from one of the two measurement periods. The blank spaces in the model coloumns for station 1, 12, 13, 14, 15, and 16 indicate that these stations are located outside the model domain, see figure 2. The measurement data for these stations are presented, however, for completeness and comparison of the results from each of two recording time-periods.

In the following pages we will present the measured current data from the 18 stations in Trondheimsleia in tables 4.3-4.3, one for each of the four tidal components M_2, S_2, N_2, and K_1, from the first period of observation (Measurement 1), the second period (Measurement 2). In the same tables HRMT model data from the model gridpoint nearest to the location of the recording station are given. For all stations both the water depth and sensor-depth are shown. A is the semi-major axis, B is the semi-minor axis, θ is the inclination and rot is the direction of rotation of the current vector. Note that $(+)$ denotes rotation in clockwise direction and $(-)$ denotes rotation in counterclockwise direction.

Table 8: Current ellipse for the M_2 constituent.

St.	*Measurement 1*					*Measurement 2*					*Model*				
	Depth m	A cm/s	B cm/s	θ deg	rot	Depth m	A cm/s	B cm/s	θ deg	rot	Depth m	A cm/s	B cm/s	θ deg	rot
1	217/220	6.82	1.05	62	−										
2	217/220	7.61	0.92	71	−	217/220	6.97	0.17	57	−	228	9.87	0.54	69	−
3	112/115	16.46	3.71	90	+	112/115	11.28	2.02	90	+	112	15.72	3.24	85	+
4	272/275	3.00	0.04	43	−						277	5.83	2.61	66	−
5	357/360	13.32	0.66	50	−	357/360	11.73	0.25	43	−	355	12.68	0.60	59	−
						357[a]	14.35	2.21	43	−					
6											408	21.10	0.62	58	−
7	407/410	23.58	0.95	151	+	427/430	19.89	0.69	139	+	370	19.31	1.19	152	+
	377[b]	21.74	1.07	152	+										
8	517/520	16.00	0.27	26	+	517/520	13.36	0.37	1	+	519	14.26	0.40	10	−
9						587/590	11.26	0.15	138	−	588	10.63	0.03	166	−
10	547/550	6.55	1.86	161	−	547/550	6.98	1.28	168	−	547	9.85	0.02	166	−
11	497/500	4.65	2.06	71	−	497/500	2.38	1.12	73	−	499	4.39	0.07	58	−
12	37/40	31.62	4.96	30	+	37/40	30.74	3.20	25	+					
13	187/190	14.15	1.00	42	+	187/190	13.03	2.36	39	+					
14	417/420	6.58	1.46	56	−	417/420	3.27	0.80	61	−					
15	197/200	2.05	0.12	30	−	217/220	0.20	0.15	33	−					
16	27/30	4.34	0.16	102	+	27/30	4.09	0.24	114	+					
17	40/80	28.23	1.36	99	−						45	43.15	10.43	113	−
18	47/50	15.71	2.57	108	−						47	38.74	8.86	165	+

[a]Depth mean values for 2nd measurement (ADCP) period
[b]Depth mean values for 1nd measurement (ADCP) period

Table 9: Current ellipse for the S_2 constituent.

St.	*Measurement 1*					*Measurement 2*					*Model*				
	Depth m	A cm/s	B cm/s	θ deg	rot	Depth m	A cm/s	B cm/s	θ deg	rot	Depth m	A cm/s	B cm/s	θ deg	rot
1	217/220	2.82	0.52	62	−										
2	217/220	2.84	0.74	47	−	217/220	3.52	0.79	44	−	228	3.37	0.19	69	−
3	112/115	6.49	0.73	94	+	112/115	4.99	0.85	86	+	112	5.41	0.99	85	+
4	272/275	1.64	1.25	172	−						277	1.99	0.95	68	−
5	357/360	7.11	0.57	49	−	357/360	6.21	0.01	43	−	355	4.61	0.20	59	−
						357[a]	6.63	0.46	62	−					
6											408	7.79	0.24	58	−
7	407/410	7.60	1.52	165	−	427/430	8.68	0.14	137	+	370	7.15	0.44	151	+
	377[b]	8.25	0.50	160	−										
8	517/520	5.85	0.66	31	−	517/520	3.38	2.49	162	+	519	5.38	0.16	9	−
9						587/590	5.58	2.02	137	−	588	3.98	0.01	167	+
10	547/550	2.95	0.74	159	−	547/550	3.73	0.81	167	−	547	3.67	0.00	167	+
11	497/500	1.86	0.73	77	−	497/500	1.10	0.52	51	−	499	1.64	0.03	57	−
12	37/40	31.62	4.96	30	+	37/40	11.51	0.84	28	+					
13	187/190	5.07	0.45	39	+	187/190	5.69	1.26	40	+					
14	417/420	2.80	0.37	53	−	417/420	1.75	0.47	59	−					
15	197/200	1.10	0.06	36	−	197/200	0.09	0.07	56	−					
16	27/30	1.65	0.10	112	−	27/30	1.82	0.31	112	+					
17	40/80	10.49	0.29	163	−						45	17.73	4.21	117	−
18	47/50	6.14	0.05	103	−						47	14.60	3.58	163	+

[a] Depth mean values for 2nd measurement (ADCP) period
[b] Depth mean values for 1st measurement (ADCP) period

[p]

Table 10: Current ellipse for the N_2 constituent.

St.	*Measurement 1*					*Measurement 2*					*Model*				
	Depth m	A cm/s	B cm/s	θ deg	rot	Depth m	A cm/s	B cm/s	θ deg	rot	Depth m	A cm/s	B cm/s	θ deg	rot
1	217/220	0.96	0.34	37	–										
2	217/220	1.32	0.68	61	–	217/220	3.25	0.64	62	+	228	2.11	0.14	70	–
3	112/115	2.92	1.42	98	–	112/115	6.37	0.69	81	+	112	3.45	0.70	85	+
4	272/275	1.47	1.14	64	–						277	1.22	0.52	63	–
5	357/360	1.50	0.15	11	–	357/360	4.16	0.01	42	–	355	2.51	0.12	59	–
						357[a]	3.84	0.16	78	–					
6											408	4.24	0.11	59	–
7	407/410	6.64	1.47	157	+	427/430	3.78	0.22	126	+	370	3.84	0.26	151	+
	377[b]	5.51	0.57	153	–										
8	517/520	3.85	0.98	41	–	517/520	4.43	1.68	29	–	519	2.90	0.12	8	–
9						587/590	3.48	0.68	150	+	588	2.14	0.02	167	–
10	547/550	1.48	0.64	153	–	547/500	1.61	0.11	160	–	547	1.96	0.01	167	–
11	497/500	1.21	0.53	63	–	497/500	1.03	0.15	49	–	499	0.82	0.02	59	–
12	37/40	6.59	0.97	28	–	37/40	5.84	0.31	31	–					
13	187/190	2.35	0.14	31	–	187/190	1.68	0.81	49	–					
14	417/420	1.39	0.32	56	–	417/420	0.78	0.28	49	–					
15	197/200	0.59	0.08	42	–	197/200	0.11	0.04	44	–					
16	27/30	0.78	0.08	107	–	27/30	0.88	0.02	104	–					
17	40/80	6.03	0.56	176	–						45	10.02	2.42	117	–
18	47/50	4.65	1.06	105	–						47	7.89	2.02	161	+

[a]Depth mean values for 2nd measurement (ADCP) period
[b]Depth mean values for 1st measurement (ADCP) period

[p]

Table 11: Current ellipse for the K_1 constituent.

St.	*Measurement 1*					*Measurement 2*					*Model*				
	Depth m	A cm/s	B cm/s	θ deg	rot	Depth m	A cm/s	B cm/s	θ deg	rot	Depth m	A cm/s	B cm/s	θ deg	rot
1	217/220	0.73	0.01	77	−										
2	217/220	1.25	0.10	55	−	217/220	1.79	0.58	42	+	228	1.21	0.13	68	−
3	112/115	2.17	0.01	88	+	112/115	1.32	0.38	42	+	112	1.76	0.88	83	+
4	272/275	0.65	0.07	168	−						277	0.75	0.23	44	−
5	357/360	0.37	0.09	55	−	357/360	0.72	0.00	23	−	355	0.62	0.03	66	−
						357[a]	0.61	0.00	150	−					
6											408	1.19	0.08	60	−
7	407/410	0.95	0.30	151	−	427/430	0.80	0.07	144	−	370	0.75	0.15	146	+
	377[b]	0.75	0.18	161	−										
8	517/520	0.78	0.14	35	−	517/520	0.38	0.09	19	−	519	0.71	0.00	1	−
9						587/590	0.41	0.10	149	+	588	0.49	0.01	169	+
10	547/550	0.47	0.07	162	−	547/550	0.21	0.05	180	−	547	0.49	0.00	169	−
11	497/500	0.39	0.02	69	−	497/500	0.10	0.04	129	+	499	0.16	0.00	56	−
12	37/40	1.36	0.30	23	+	37/40	0.82	0.17	31	−					
13	187/190	0.88	0.00	57	+	187/190	0.71	0.02	46	−					
14	417/420	0.40	0.04	16	+	417/420	0.30	0.07	44	−					
15	197/200	0.43	0.00	42	+	197/200	0.09	0.01	121	−					
16	27/30	0.37	0.14	117	−	27/30	0.20	0.02	90	−					
17	40/80	0.82	0.18	139	−						45	2.34	1.66	145	−
18	47/50	0.97	0.67	90	−						47	1.55	0.71	164	+

[a]Depth mean values for 2nd measurement (ADCP) period
[b]Depth mean values for 1st measurement (ADCP) period

5 Depth profiles of currents

ADCP measurements from station 5 and 7 (Fig. 2) are presented in the report of Krug (2002). These data provide a vertical profile of the tidal currents. By running harmonic analysis, the parameters of the current ellipse can be calculated for each tidal constituents. In Figures 6, 7, 8, and 9 plots and tables showing the depth variation of the major and minor half axes are presented for the M_2, S_2, N_2 and K_1 components.

The plots show a complex vertical variation of the half axis through the vertical water column and indication that stratification effects are important. As we see in Figure 6 that both for the M_2 S_2 constituent, the major half axes reach the maximum value in the middle of the water column.

Depth (m)	*A (cm/s)*	*B (cm/s)*
47	7.47	1.38
67	11.32	2.55
87	13.24	1.18
107	15.51	0.07
127	18.23	1.29
147	20.27	2.08
167	20.51	2.26
187	19.28	1.93
207	17.61	1.59
227	15.86	1.29
247	14.21	0.86
267	12.50	0.62
287	11.22	0.85
307	10.58	1.33
327	10.00	1.83
357	11.73	2.16

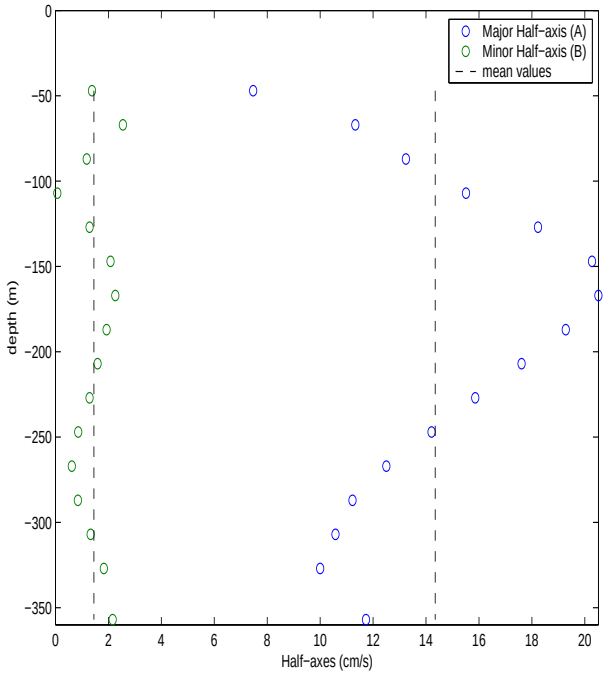

Depth (m)	*A (cm/s)*	*B (cm/s)*
47	6.21	0.39
67	5.54	0.31
87	6.18	0.38
107	6.50	0.42
127	6.71	0.45
147	7.02	0.49
167	7.37	0.54
187	7.70	0.59
207	8.10	0.66
227	8.17	0.67
247	8.23	0.68
267	7.69	0.59
287	6.67	0.44
307	5.59	0.31
327	4.83	0.23
357	3.56	0.13

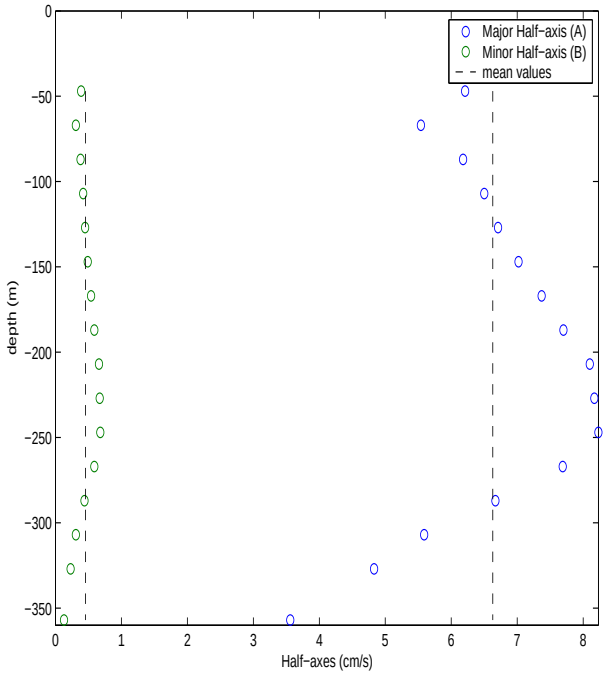

Figure 6: Measured major (A) and minor (B) half axis at Station 5. M_2 constituent at the top, S_2 at the bottom.

Depth (m)	*A (cm/s)*	*B (cm/s)*
47	4.15	0.17
67	2.73	0.07
87	3.40	0.12
107	4.06	0.16
127	4.62	0.21
147	4.75	0.23
167	4.53	0.20
187	4.67	0.22
207	4.98	0.25
227	4.88	0.24
247	4.20	0.18
267	3.88	0.15
287	3.41	0.12
307	3.06	0.09
327	2.45	0.06
357	1.74	0.03

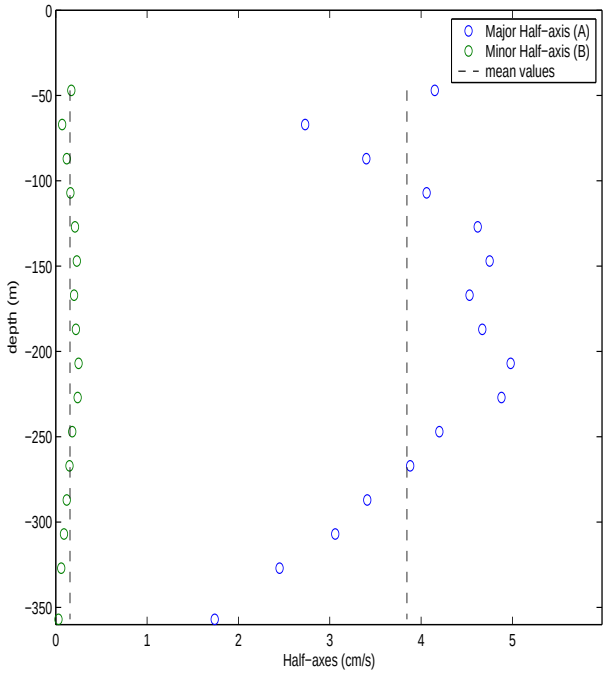

Depth (m)	*A (cm/s)*	*B (cm/s)*
47	0.72	0.01
67	0.26	0.00
87	0.28	0.00
107	0.30	0.00
127	0.36	0.00
147	0.42	0.00
167	0.74	0.00
187	0.35	0.00
207	0.70	0.00
227	0.86	0.01
247	0.65	0.00
267	0.48	0.00
287	0.42	0.00
307	0.39	0.00
327	0.51	0.00
357	2.30	0.05

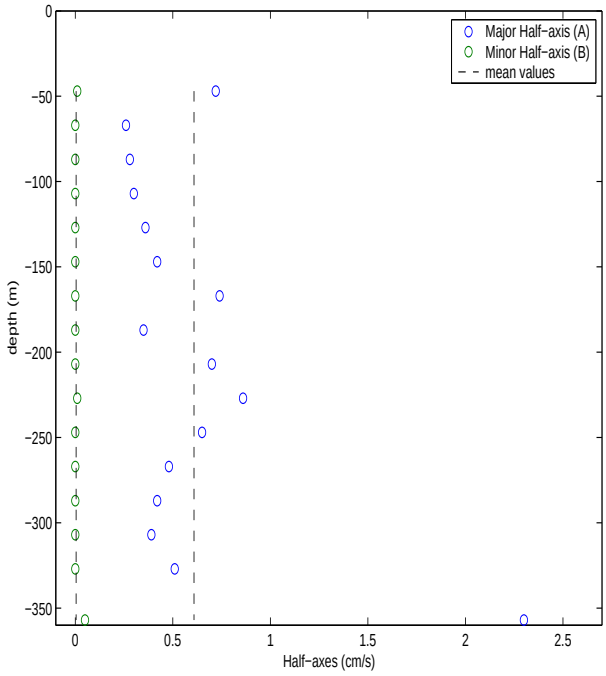

Figure 7: Measured major (A) and minor (B) half axis at Station 5. N_2 constituent at the top, K_1 at the bottom.

Depth (m)	*A (cm/s)*	*B (cm/s)*
37	12.99	0.21
67	15.24	0.67
77	16.63	1.07
97	17.36	0.37
117	18.27	0.80
137	19.82	1.14
157	21.66	0.42
177	23.65	0.81
197	25.23	1.52
217	25.77	1.58
237	26.83	0.93
257	26.68	0.04
277	26.34	0.94
297	26.35	1.66
317	26.19	2.05
337	24.89	2.09
357	22.25	1.88
377	15.10	1.07

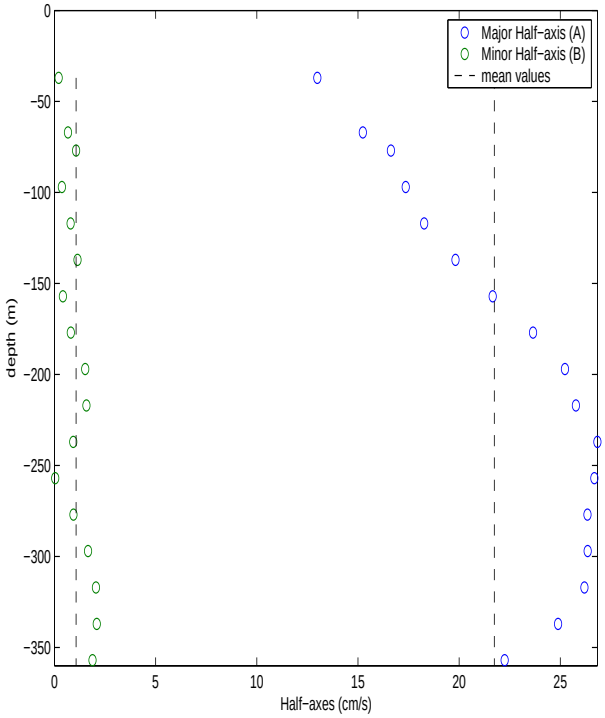

Depth (m)	*A (cm/s)*	*B (cm/s)*
37	5.64	0.05
67	6.01	0.36
77	4.38	0.01
97	6.66	0.41
117	7.19	0.84
137	8.28	1.01
157	9.39	0.44
177	10.25	0.09
197	10.41	0.22
217	10.05	0.03
237	10.28	0.23
257	10.16	0.37
277	9.97	0.62
297	9.81	0.87
317	9.35	1.08
337	8.55	0.96
357	7.34	0.77
377	4.82	0.66

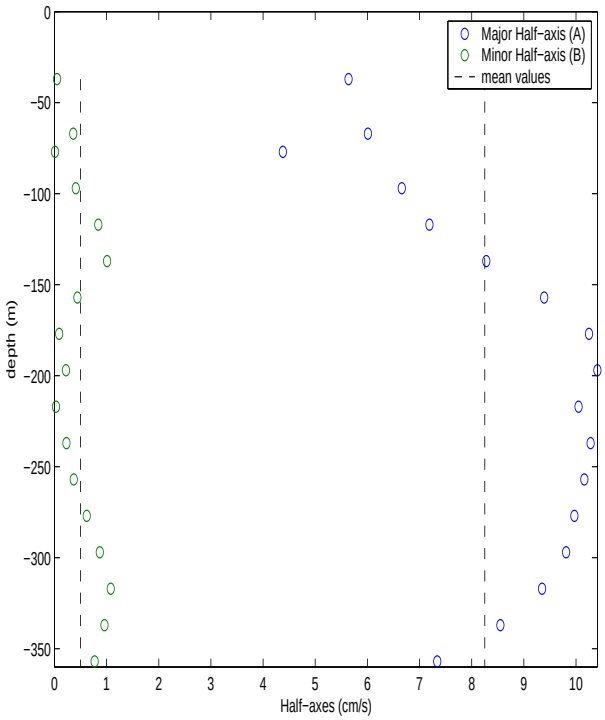

Figure 8: Measured major (A) and minor (B) half axis at Station 7. M_2 constituent at the top, S_2 at the bottom.

Depth (m)	*A (cm/s)*	*B (cm/s)*
37	3.22	0.41
67	3.24	0.23
77	3.16	0.48
97	3.58	1.05
117	4.62	0.76
137	5.19	0.45
157	5.57	0.32
177	5.68	0.52
197	5.92	0.82
217	6.20	0.77
237	6.61	0.73
257	6.70	0.59
277	6.77	0.43
297	6.96	0.41
317	7.18	0.47
337	7.19	0.59
357	6.80	0.69
377	4.80	0.57

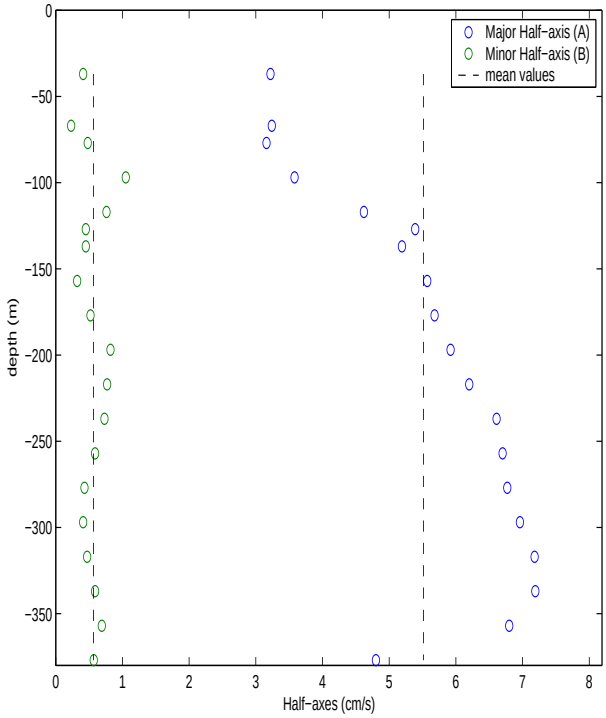

Depth (m)	*A (cm/s)*	*B (cm/s)*
37	0.53	0.21
67	0.57	0.01
77	0.66	0.01
97	0.60	0.16
117	0.62	0.04
137	0.75	0.30
157	0.96	0.45
177	1.06	0.29
197	0.88	0.16
217	0.73	0.25
237	0.75	0.32
257	0.85	0.34
277	0.83	0.33
297	0.82	0.15
317	0.81	0.04
337	0.66	0.01
357	0.69	0.05
377	0.66	0.06

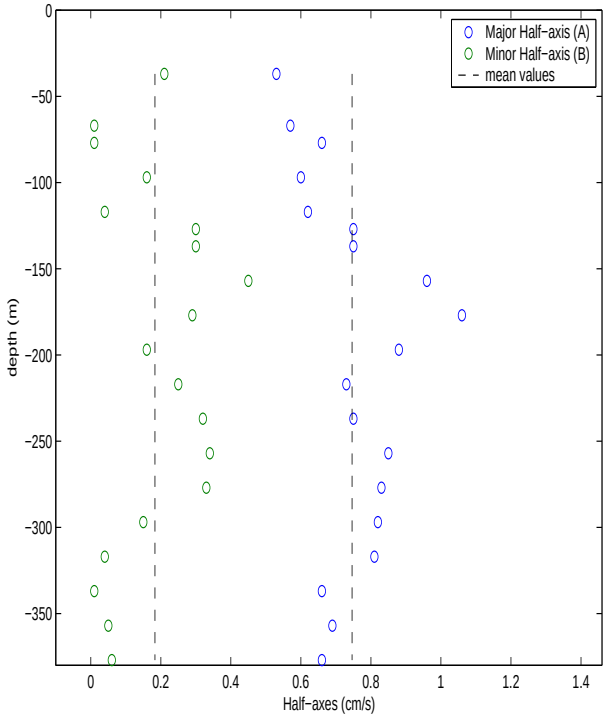

Figure 9: Measured major (A) and minor (B) half axis at Station 7. N_2 constituent at the top, K_1 at the bottom.

6 Short periodic oscillations

The analysis of the RCM data from stations 17 and 18 located in the channel between the island Storfosna and Ørlandet on the main land (see Figure 2 and Figure 3), revealed some interesting results. Particularly at station 17 bursts of short periodic oscillations of variable amplitude appeared episodically throughout the whole period of observation.

These oscillations are especially strong at spring tide and most pronounced in the East-West component of the current at the time when the current speed is near maximum in the South direction. The observed tidal currents for the whole measurement period are shown in Figure 10. We have used Julian calender-days for the time axis on these plots. This calender starts at the 1st of January and the 32th day in the Julian calender system is 1 February.

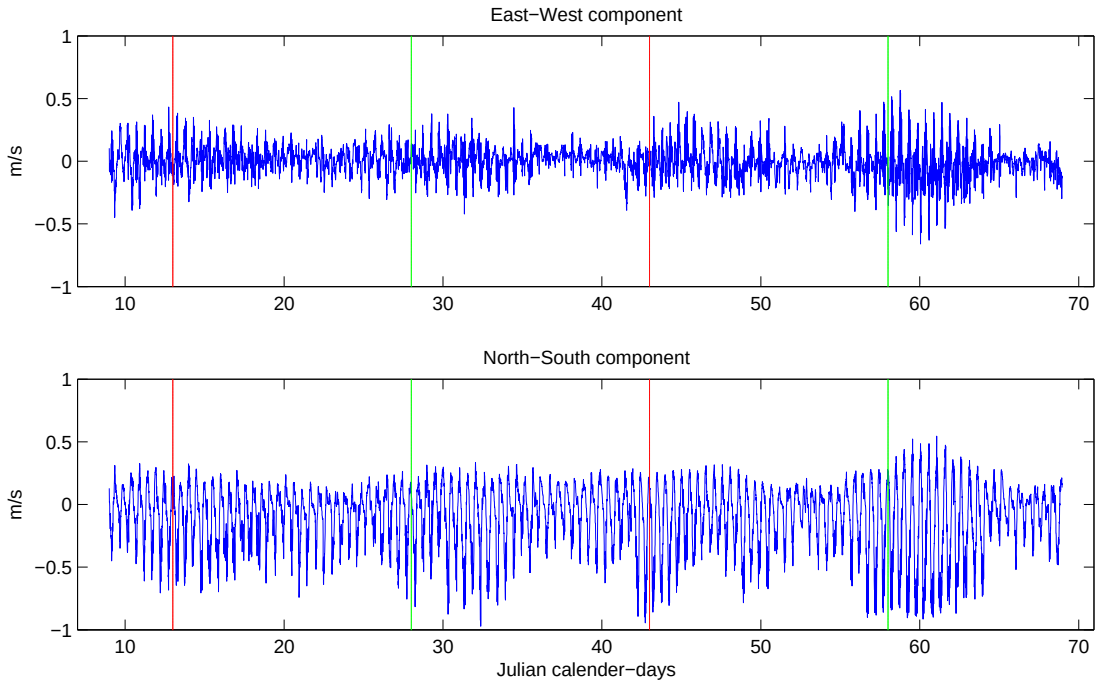

Figure 10: The RCM measurements from 9th of January to 10th of March 2002. Red line indicates full-Moon, green line indicates new-Moon. Current components are reckoned positive towards north and east, respectively.

To illustrate this phenomena, we consentrate here on shorter intervals of the measurement period. Figure 11 shows the period 26th to 28th of February, around the time of full Moon which occured 27th February (Julian day 58) and coincided nearly with lunar perigee. Throughout the entire period of measurement, these two days had the strongest current both in North-South and East-West direction. The current in the South direction reached speeds at almost 1 m/s. Fig. 12 show a close up of the time series with the oscillation on Julian day 57. Figure 13 illustrates the behaviour in the current phase plane at time intervals where the south component is large. It is noticeable that the curves describes a rotational behaviour in anticlockwise directions at all of these periods. The left panel in the plots shows linear interpolated values, while the right panel shows spline interpolation. Another period with

energetic oscillations is from the 12th of January to the 14th of January coinciding with new Moon 13 January (Fig. 14).

Figure 15 covers a period of 2 days from the 21th of January (Julian day 21), a period with half Moon and weak tidal current. In this and other intervals where the oscillation are almost absent, the North-South component is relatively small (a magnitude of approximately 0.3-0.5 m/s).

The maximum current speed is less at station 18 than at station 17, and the short periodic oscillations are less evident (Fig 16). Calculations show that the period of the oscillations at station 17 varies between 36 to 48 minutes, see Table 6.

These oscillations are either small scale eddies structure shedded from topographic features near station 17 or eddies formed by shear flow instability of the main tidal jet through the channel.

To investigate the first hypotesis we use the Strouhal number relation

$$S = \frac{nd}{U} = 0.2 \tag{2}$$

where $n = \frac{1}{T}$ is the frequency and T are the period of the oscillations, d is the diameter of the eddy shedding object and U is the typical current speed past the object. With T= 40 min and U = 0.5 m/s we obtain d= 240 m. Figure 3 shows that there is a pronounced topographic features of comparable size west of station 17. However, if there is systematic eddy shedding from this feature one would also expect to see the oscillations at station 18 and the new additional station located between 17 and 18 (see section 7). Since there is little evidence of regular oscillations similar to what we see at station 17 in the data sets from the two other stations we find it unlikely that the oscillations are caused by the topographic feature west of station 17.

Therefore, the other hypotesis; oscillations caused by shear flow instability is the most likely mechanism. In a Ms-thesis by Aakervik (2004), stability of a tidal jet was investegated through a narrow sound or channel, as near station 17 and 18, and found indeed that eddies were generated and advected downstream in the shear flow. The frequency of the eddy induced oscillation was of the same order as observed. The numerical experiments were made with a model with an idealized flat bottom topography. An obvious extention would be to use the real topography for the model simulation.

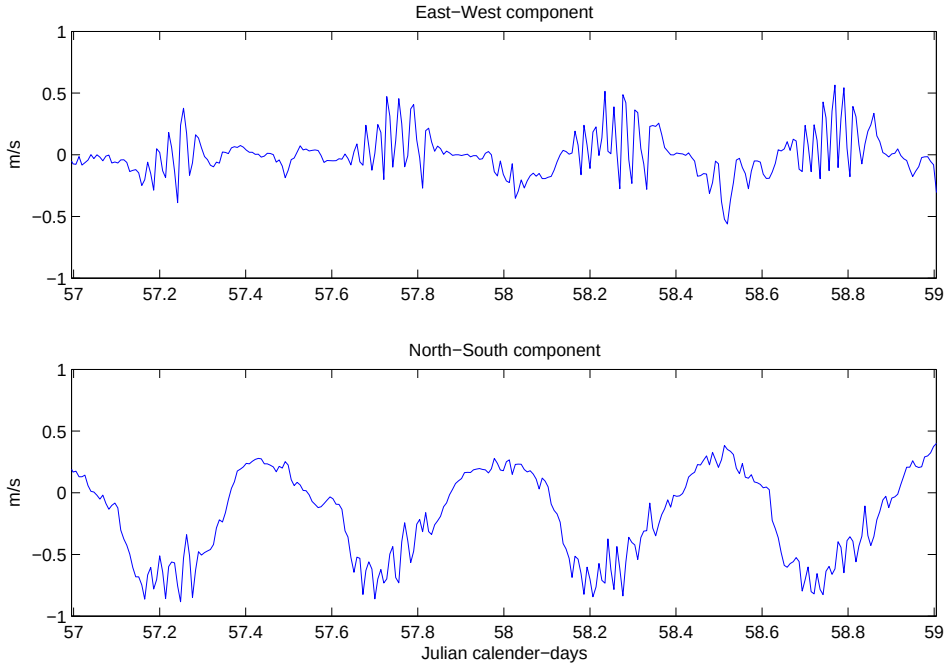

Figure 11: Close up of Figure 10; RCM measurements from the 26th to 28th of February (57th to 59th in the Julian calender). Notice the systematic oscillations in the east-west component coincing with strong south current.

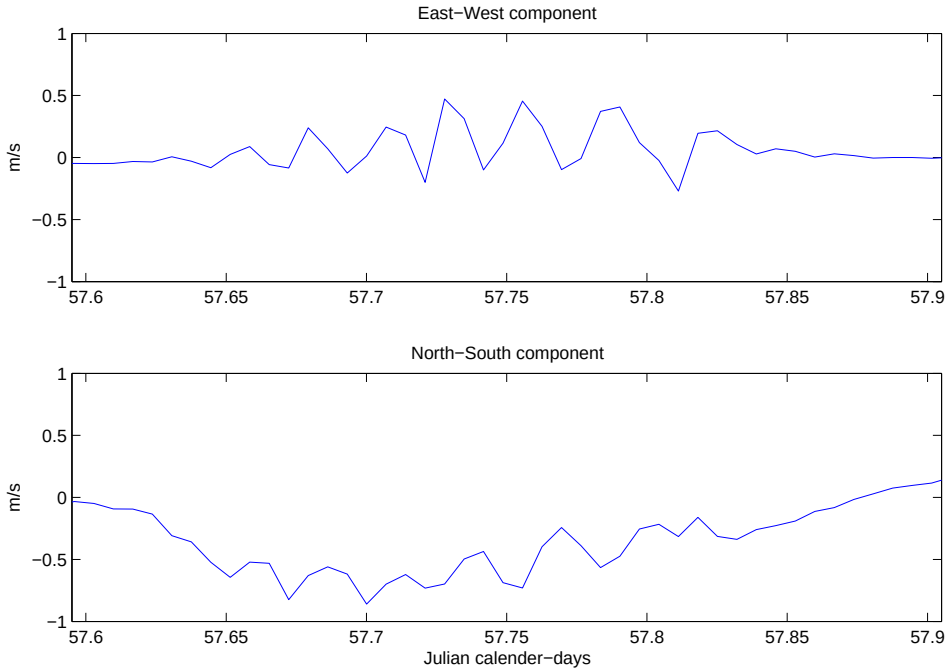

Figure 12: Close up of Figure 11; the short periodic oscillations occuring at the 26th of February (Julian day 57).

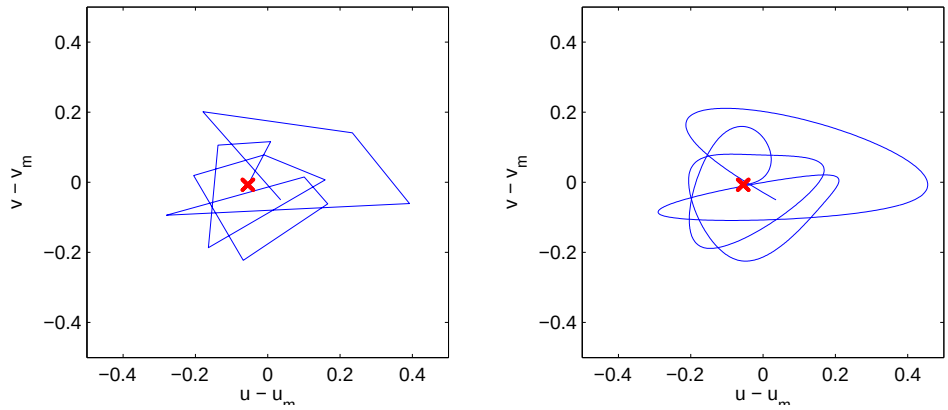

Figure 13: Phase plane plot of current vector from day 57.65-57.75 Julian day. Left: linear interpolation, Right: spline interpolation. Current components are relative to mean current (u_m, v_m).

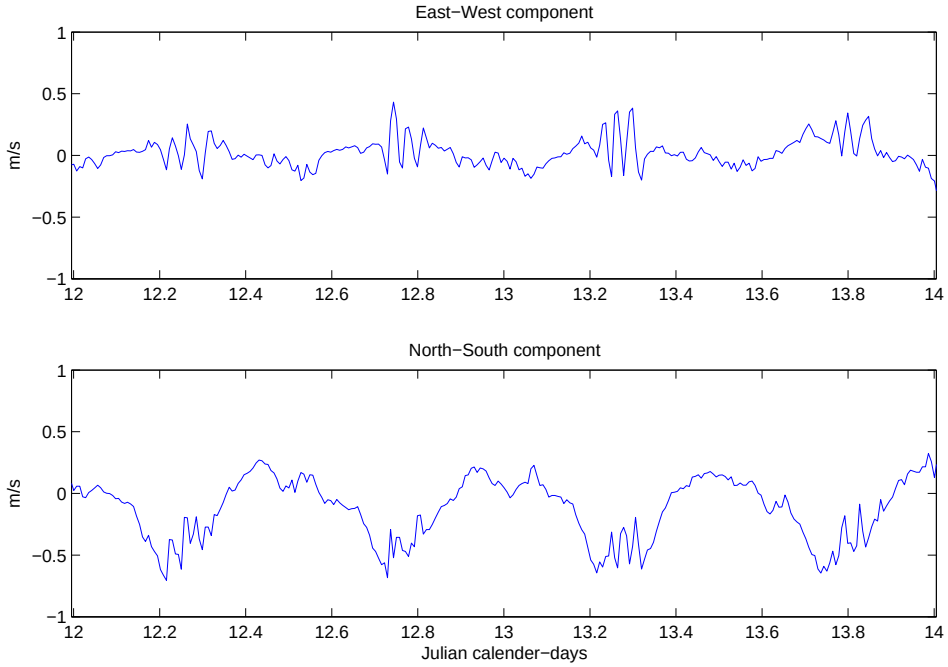

Figure 14: Observed currents at station 17, on 12. - 14. January 2002 (Julian days 12 - 14). Full Moon 13. January.

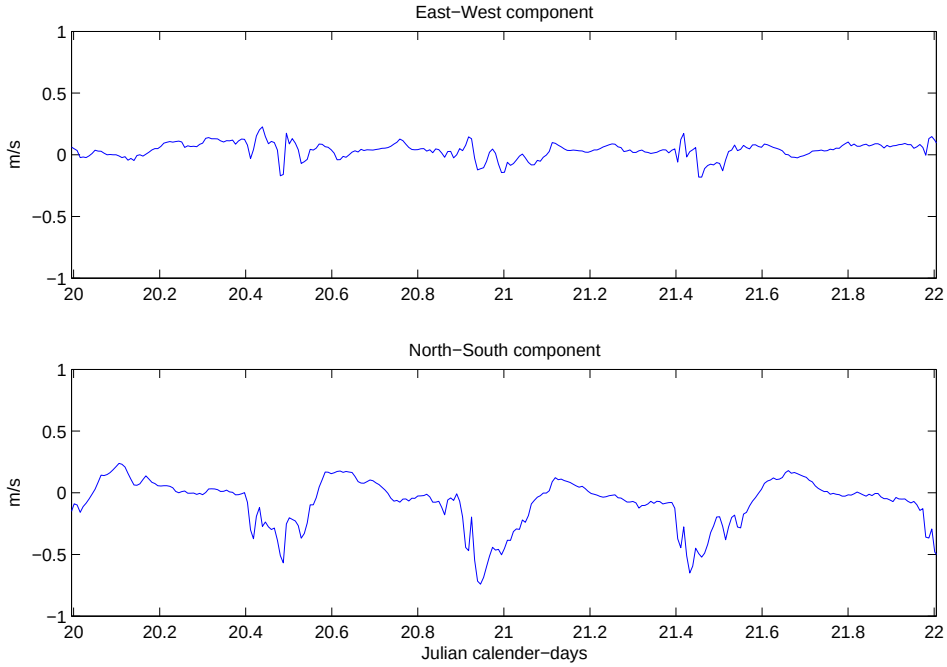

Figure 15: Half-moon, station 17.

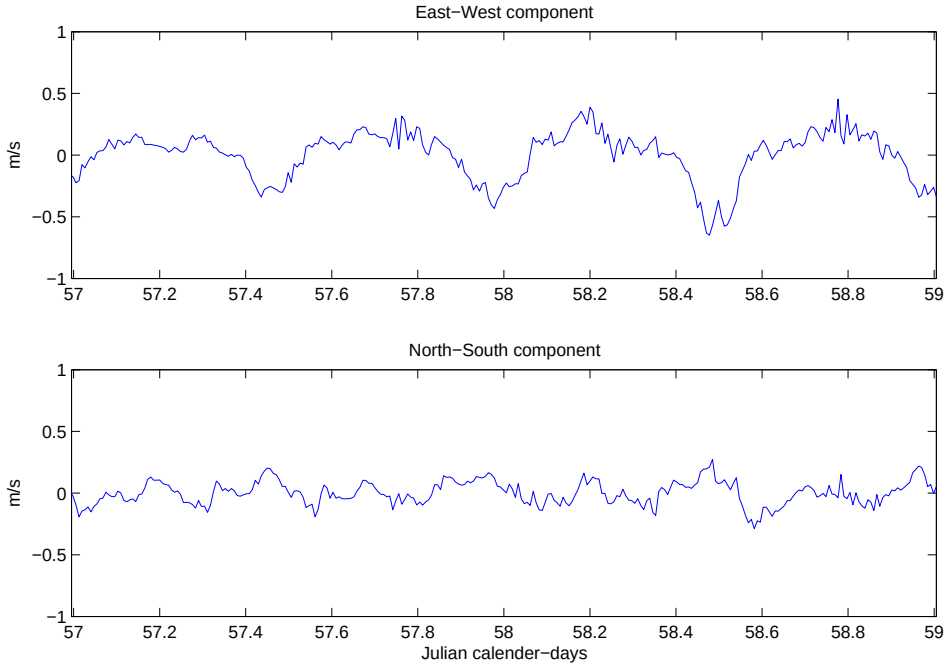

Figure 16: New-moon, station 18.

Table 12: Periods and amplitudes of short periodic current oscillations at station 17. Amplitudes are measured from trough to crest.

Julian days	*Number of oscillations*	*Period min*	*Amplitude m/s*
12.74 - 12.84	3	48	0.58
13.22 - 13.33	4	40	0.55
30.20 - 30.40	6	48	0.63
42.70 - 42.85	5	43	0.40
43.15 - 43.35	6	48	0.66
57.15 - 57.30	5	43	0.75
57.65 - 57.85	7	41	0.69
58.15 - 58.40	8	45	0.78
58.70 - 58.80	4	36	0.72
61.20 - 61.40	8	36	0.57
61.75 - 61.95	7	41	0.51

7 Recent current measurements

In the period 23. November 2003 to 4. April 2004 the Norwegian Defense Research Establishment (FFI), Horten, conducted ADCP measurements at a station in the channel between Storfosna and Garten near the former stations 17 and 18, see fig 17. The UTM-coordinates for this station was 524137 E and 7055949 N, and the water depth was approximatly 40 m. The currents (both horisontal and vertical) was sampled with 5 minutes intervals at three depth level; 10, 20 and 30 metres above the sea bed.

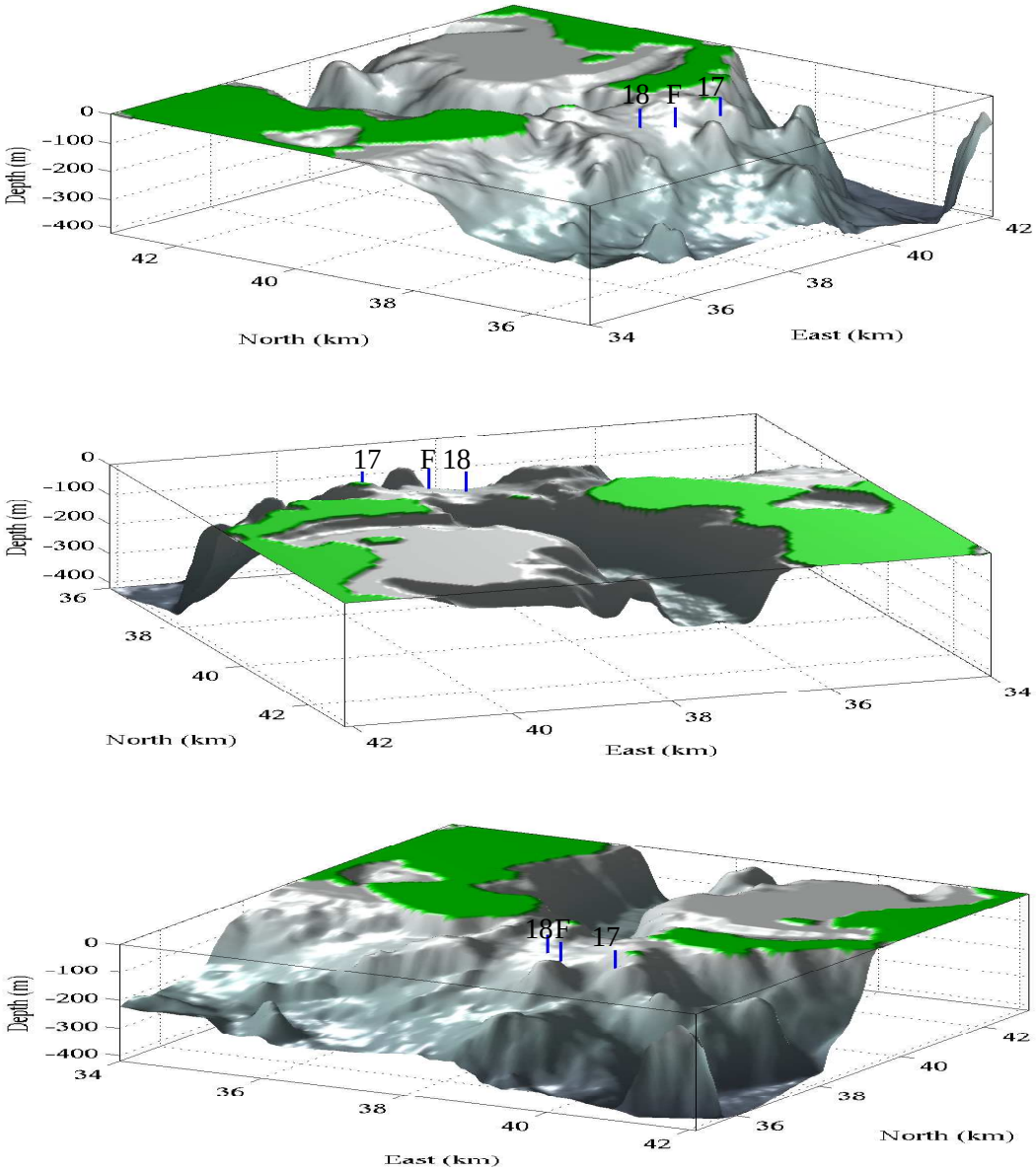

Figure 17: 3-D plots of the bottom topography around stations 17, 18 and the new FFI station from different views (FFI station marked with an "F").

An example of the recorded time series is shown in fig 18 covering the periods of two days from 8th of March to 10th of March. A blown up sequence of about 10 hours from the same series is shown in fig 19.

The plots in fig 18 and 19 show that there generally is a smale increase in current speed from the lower to the upper level. It is also seen that the records contain high frequency oscillations, but there does not seems to be regular bursts of short periodic oscillations as found in the data from station 17. The data from this station will be analysed in more details in the future.

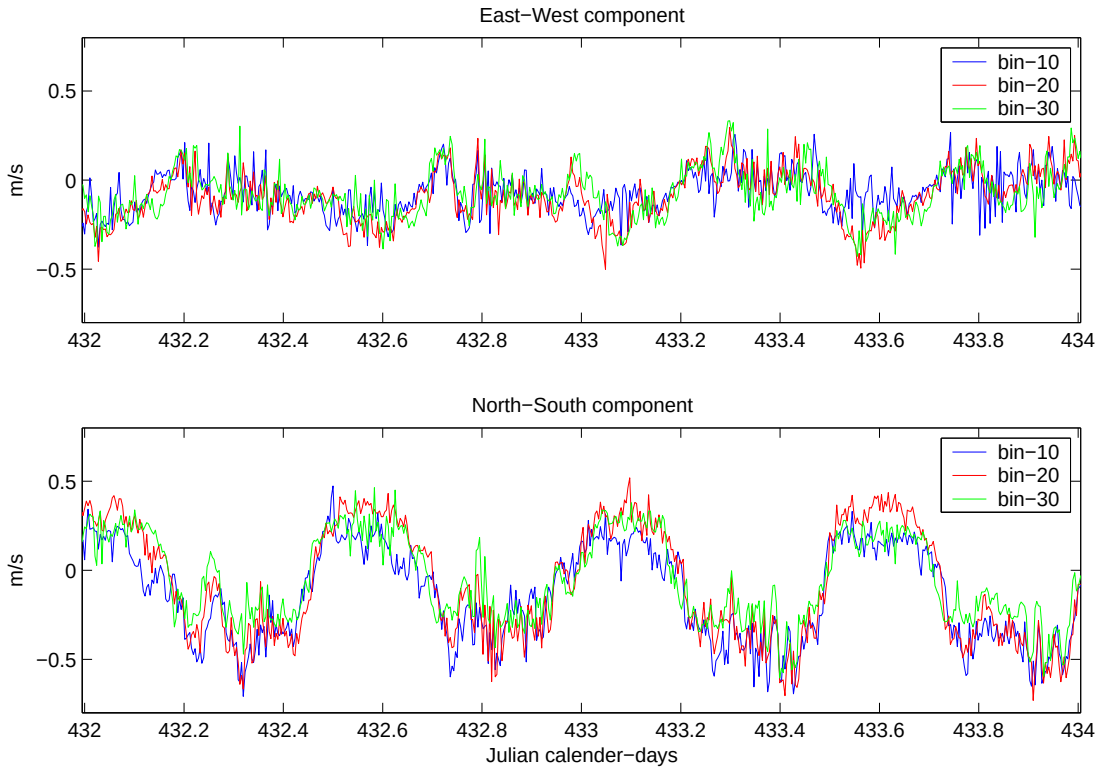

Figure 18: Current measurements made by FFI. Bin 10 is set 10 metres above the bottom, Bin 20 is 20 metres above the bottom, and Bin 30 is 30 metres.

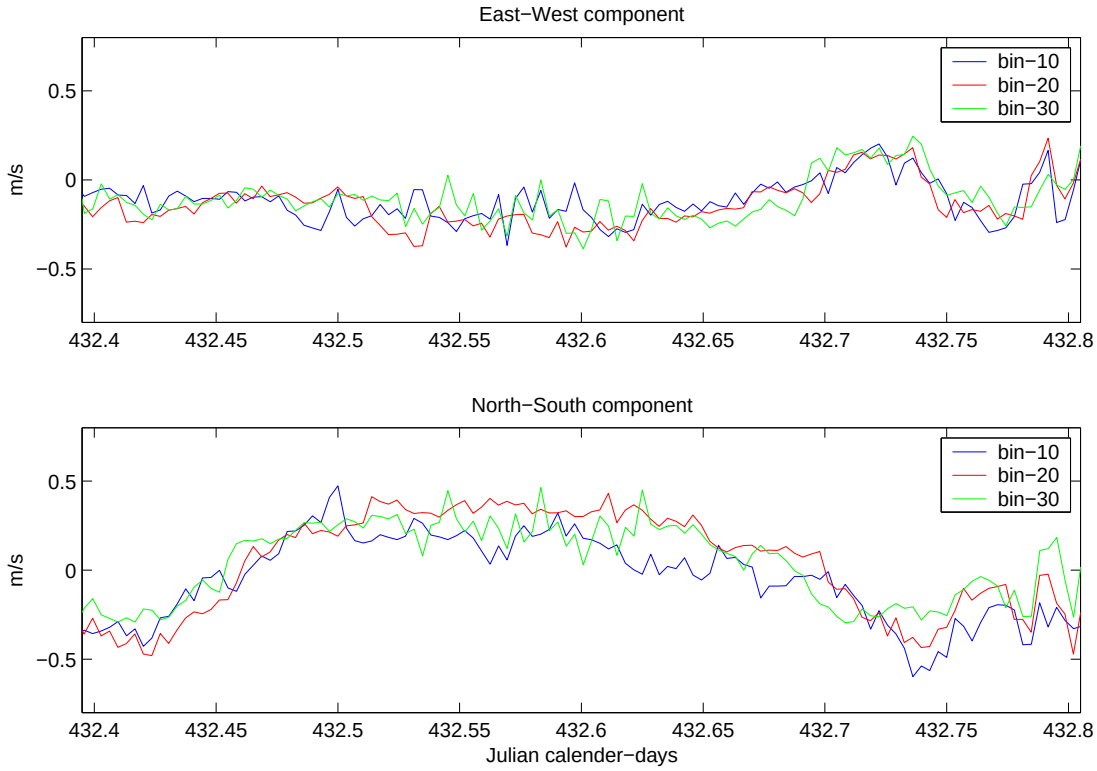

Figure 19: Close-up of Figure 18

8 Concluding remarks

The modelled sea level data are found to agree very well with observations. For the current data the agreement is reasonable and the model clearly predicts the main spatial variability of the current field. The fact that most of the current measurements available are made close to the sea bed while the model predicts depth mean values restricts the possibility to validate the model. The new data briefly described in section 7 has to be analysed in more detailed before comparison with the model data.

Acknowledgement

We are gratefull to E. Nygard at Statoil, Stavanger, and J. K. Jensen at FFI, Horten, for being given access to the observational data.

References

Aakervik, E. (2004), Testing av ulike skjema for simulering av tidevatnsstraumen i straumsterke sund, Master's thesis, Department of Mathematics, University of Oslo.

Gjevik, B. (2001), 'Lectures on tides'. http://www.math.uio.no/~ bjorng/svalbard_unis/.

Gjevik, B., Hareide, D., Lynge, B., Ommundsen, A., Skailand, J. & Urheim, H. (2004), 'Implementation of high resolution tidal current fields in electronic charts systems', *Marine Geodecy* . Submitted, sub judice.

Hareide, D. & Lynge, B. (2002), Water level observation from Trondheimsleia and Frohavet, Technical report, Norwegian Mapping Authority, Hydrographic Service.

Krug, M. (2002), Current Measurements Offshore Norway, Technical report, Thales Geosolutions.

Moe, H., Gjevik, B. & Ommundsen, A. (2003), 'A high resolution tidal model for the coast of Møre and Trøndelag, Mid Norway', *Norwegian Journal of Geography* **57**(65-82).

Orre, S. (2004), Kaotisk transport og miksing av partikler i kystnære tidevannsfelt, Master's thesis, Department of Mathematics, University of Oslo.

Xing, J. & Davies, A. (2003), A 3-D Tidal Model of Trondheimsleia Channel: Some Preliminary Results. Presentation Oslo 15/5 2003.

Xu, Z. (2002), Ellipse parameters conversion and vertical velocity profiles for tidal currents, Technical report, Bedford Institute of Oceanography, http://sea-mat.whoi.edu/tidal-ellipse-html/index.html.